Fractal Character of the Auditory Neural Spike Train

MALVIN C. TEICH, FELLOW, IEEE

Abstract—**Long-counting-time pulse-number distributions (PND's) were measured from a broad variety of cat primary auditory fibers using different tone and noise stimuli, counting times T, and number of samples N_T. Whereas short-counting-time PND's ($T \sim 50$ ms) manifest the presence of spike pairs (an enhancement of even- over odd-count probabilities), the irregular shapes of the long-counting-time PND's ($T \gtrsim 0.1$ s) reveal that the underlying sequence of action potentials consists of spike clusters when viewed on a longer time scale. For all units measured, the count variance-to-mean ratio (Fano factor) $F(T)$ varied little over some 90 dB change in the stimulus level. On the other hand, $F(T)$ increased substantially as T and/or N_T were increased, corresponding to the capture of larger and larger spike clusters in the counting time. A relationship is developed between the Fano-time function $F(T)$ and the normalized coincidence rate function, $g(\tau)$ versus delay time τ. A plausible form for $g(\tau)$ leads to a Fano-time function in good accord with the data. The observed power-law growth of the Fano factor for large counting times [$F(T) \sim T^{\alpha}$ where $0 < \alpha < 1$] is accompanied by a power-law decay of the coincidence rate for large delay times [$g(\tau) \sim \tau^{\alpha - 1}$] and a power-law form for the power spectral density at low frequencies [$S(f) \sim f^{-\alpha}$]. The behavior of the PND's and the scale invariance implicit in these fractional-power-law relationships suggest that the neural events on all primary auditory fibers exhibit fractal behavior for sufficiently large times (sufficiently low frequencies). The spike pairs and spike clusters in the PND's are natural consequences of this behavior. The fractal dimension $D \equiv \alpha$ is estimated to be in the range of $0.3 \lesssim D \lesssim 0.9$ for counting times in the range 0.1–10 s. The fractal dimension provides a measure of the degree of event clustering, or irregularity of a sequence of events, that is preserved over different time scales. PND's from low-skew vestibular units, in contrast, do not exhibit fractal behavior. It is suggested that auditory neural-firing patterns may serve to efficiently sample natural fractal noises.**

I. Introduction

In a recent paper [1], we emphasized the importance of characterizing neural activity in a peripheral auditory nerve fiber in terms of a stochastic point process. The term "point process" designates a sequence of times (e.g., neural-spike[1] registrations) at which events occur [2]. Identifying a point process from a stream of data is a difficult task. Because the number of occurrence times is large, it is customary to begin the process by extracting several kinds of partial statistical data from the sequence of times. As examples, measures such as the pulse-interval distribution (PID), poststimulus time histogram (PST), and pulse-number distribution (PND) may be constructed. The PND is the probability $p(n, T)$ of observing n neural spikes in the counting time T, versus the number of spikes n [1]. Other measures of interest include the joint and conditional probability densities of multicoincidence; the joint densities of forward-recurrence, backward-recurrence, and interevent (pulse-interval) times; and the joint densities of numbers of events in a sequence of time windows.

Each such measure provides its own *partial* information about the underlying spike train. The PID, for example, is a histogram formed from the times between successive events [3]. As such, its statistical accuracy is greatest for data close to the mean interspike-interval time. Interspike intervals that are long compared to the mean appear in the tail of the distribution. Thus, there are few of them and their statistical accuracy is poor. The PST histogram (or period histogram) is constructed by averaging the neural spikes modulo a stimulus unit cell [4]. It is a measure that is therefore phase-locked to (or synchronous with) the stimulus. The PND, on the other hand, is an asynchronous measure since the time T is related neither to the stimulus nor to the spike train. The counting time T, which is externally specified, determines the time over which correlations in the neural spike train may be observed in the PND [5].

Of the three measures most commonly used to investigate a neural spike train (the PST, PID, and PND), the PND lends itself most naturally to the study of long-time spike correlations [1]. Ideally, it is desirable to experimentally collect a sequence of PND's, each with a different value of T, to provide the greatest detail about the underlying structure of the sequence of action potentials.

In our initial investigation of this topic, we examined the behavior of the PND from primary afferent auditory fibers for a relatively short ($T = 51.2$ ms) counting time [1]. The scalloped character of some of these PND's led us to recognize that closely occurring spike pairs were often present in the underlying action-potential sequence. This prompted us to examine the behavior of the spike train over a longer time period. A follow-up study of the PND [6], in which we used a counting time $T = 204.8$ ms, revealed rather irregular distributions indicating the presence of clusters that often contained more than two spikes. It became apparent that although the short-counting-time PND's [1] and the long-counting-time PND's [6] were constructed from the same underlying spike trains, the different values of T provided complementary information about the underlying neural spike train.

Manuscript received January 27, 1988; revised August 8, 1988. This research was supported by the National Science Foundation and by the National Institutes of Health.

The author is with the Center for Telecommunications Research, Department of Electrical Engineering, Columbia University, New York, NY 10027 and with the Fowler Memorial Laboratory, Department of Otolaryngology, Columbia College of Physicians & Surgeons, New York, NY 10032.

IEEE Log Number 8824426.

[1]The terms "neural spike," "pulse," and "action potential" are used interchangeably.

The irregularities in the PND's were found to increase with increasing counting time, revealing a hierarchy of correlated spike occurrences extending over multiple time scales. The clusters manifested in short counting-time PND's turn out to be subclusters of larger clusters, which appear in PND's with longer counting times, and so on, in nested fashion. The spike pairs evident in the short-counting-time PND's are the smallest subclusters that are observable; the production of tighter subclusters is limited by refractoriness in the nerve fiber. The irregularities in the PND's were also found to increase with increasing sample number.

These and other observations provide evidence that, above the lower limit set by refractoriness (called the inner cutoff), the auditory neural spike occurrences behave as a fractal sequence of events. The fractal dimension D is estimated to lie in the range $0.3 \lesssim D \lesssim 0.9$. The fractal dimension [7] provides a measure of the degree of event clustering [8], or irregularity of a sequence of events, that is preserved over different time scales. As a counterpoint to this behavior, it is shown that the neural spike train on peripheral vestibular fibers does not exhibit fractal behavior ($D = D_T = 0$).

An abbreviated version of the results reported here was presented at the Annual Meeting of the Acoustical Society of America in Honolulu, Hawaii in November 1988 [9].

II. Results

A. Methods

Pulse-number distributions (PND's) were recorded from primary afferent fibers in the auditory nerve of anesthetized cats, using standard extracellular microelectrode recording techniques. Pure-tone and broadband-noise stimuli were used. The methods used in our experiments, including the surgical preparation and equipment, were described earlier [1].

Various statistics of the PND, namely the count mean $\langle n(T) \rangle \equiv M$, count variance $\sigma^2(T) \equiv V$, count mean-to-variance ratio, $R(T) \equiv R$, and its reciprocal the count variance-to-mean ratio $F(T) \equiv 1/R$, can be calculated. M and $F(T)$ [or $R(T)$] provide useful measures of the PND in compact form. They are often more useful than the individual probabilities that comprise the PND since they are measures of the distribution as a whole. They provide statistically significant evidence that the short- and long-counting-time PND's contain different information.

B. PND Statistics

A representative set of PND data for $T = 204.8$ ms is provided in Fig. 1. PND's for this high-spontaneous, low-frequency unit are shown in Fig. 1(a)–(h) for pure-tone stimuli with frequencies $f_T = 371$ Hz [(a), (e)]; $f_T = 625$ Hz at the characteristic frequency (CF) of the unit [(b), (f)], and $f_T = 918$ Hz [(c), (g)]. These represent the probabilities $p(n, T)$ of observing n spikes in the counting time T, displayed as a function of n. Each PND shown consists of $N_T = 250$ samples. The sound pressure levels (relative to the frequency tuning curve [1], in (a)–(c) were: −20 dB (solid curves), 0 dB (dashed curves), and +20 dB (dotted curves). The sound pressure levels in (e)–(g) were: +30 dB (solid curves) and +50 dB (dashed curves). For the noise stimuli in (d) the sound pressure levels were approximately −50 dB (solid curve), −30 dB (dashed curve), and −10 dB (dotted curve), and in (h) they were approximately 0 dB (solid curve) and +20 dB (dashed curve). Short-counting-time PND's constructed from the same spike train were presented in [1, Fig. 4]. The frequency tuning curve (FTC) for this unit is shown in [1, Fig. 3].

The conversion of the above-specified values of dB : re FTC into values of dB SPL (re: 0.0002 dyne/cm^2) requires adding the sound-pressure value at the FTC. Since the threshold for this unit (at CF) is 23 dB SPL, the absolute stimulus levels for the data in (b), (f) are obtained by adding 23 dB. Thus, in (b) the solid, dashed, and dotted curves correspond to +3, 23, and 43 dB SPL, respectively. In (f) the solid and dashed curves correspond to +53 and 73 dB SPL, respectively. The absolute stimulus levels in (a), (e), (c), (g) are yet 15 dB higher since these frequencies were chosen at points on the FTC that are 15 dB above its minimum.

Experimental results for the long-counting-time PND count mean (dotted curve, denoted M), count variance (dash-dot curve, denoted V), and count mean-to-variance ratio (solid curve, denoted R) are presented in (i) for $f_T = 371$ Hz, in (j) for 625 Hz (CF), in (k) for 918 Hz, and in (l) for noise. The abscissa represents dB : re FTC. The point marked S represents the absence of external stimulus (spontaneous counts) and the tic marks represent 10 dB increments (the left-most tic mark represents −20 dB, except for a noise stimulus in which case it represents −50 dB). The curves denoted M are proportional to the usual spike rate function.

The mean of the $T = 204.8$ ms PND is precisely four times the mean of the $T = 51.2$ ms PND for all stimulus levels, indicating that the mean scales proportionately with T in this counting-time region. The variance, however, does not scale in this simple linear manner. However, the count mean and variance for PND's collected with $T = 204.8$ ms both increase with stimulus level in such a way that the variance-to-mean ratios turn out to be remarkably independent of stimulus level and frequency (the mean-to-variance ratio R is shown in Fig. 1). This is true for all four of the stimuli. It is also the case for the $T = 51.2$ ms results reported previously [1]. For both sets of data, there appears to be a slight trend toward decreasing $F(T)$ (increasing R) with increasing stimulus level. For short-counting-time PND's, with $N_T = 1000$, we found [1] that the typical range adopted by most (but not all) primary fibers, over the 90 dB range of applied stimulus level, was $\frac{1}{2} \leq F(T = 51.2 \text{ ms}) \leq 1$ ($1 \leq R \leq 2$). Units generating visible spike pairs tended to fall toward the higher end of this range of F. For long-counting-time experiments, with $N_T = 250$, the range of $F(T)$ extends a bit higher; typically $\frac{1}{2} \leq F(T = 204.8 \text{ ms}) \leq 2$ ($\frac{1}{2} \leq$

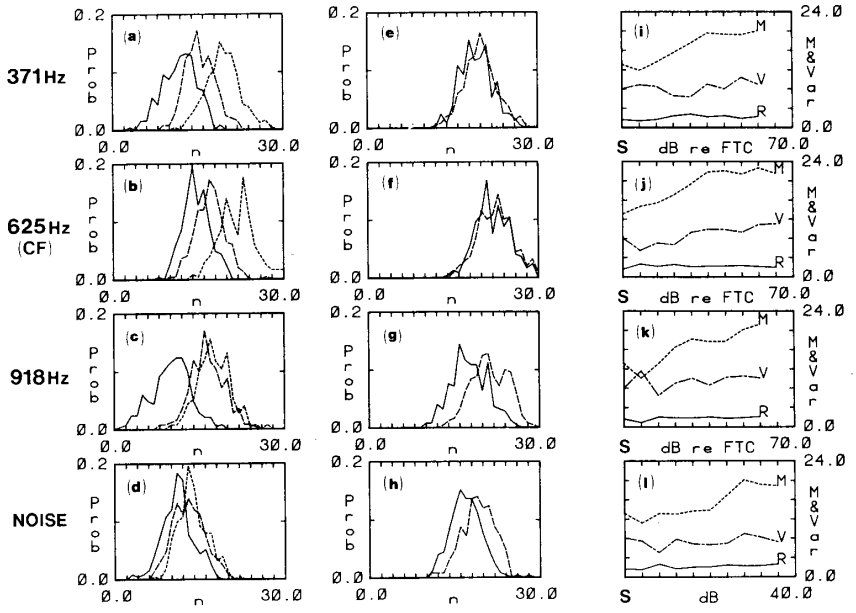

Fig. 1. Long-counting-time pulse-number distributions (PND's) for a high-spontaneous (63.9 counts/s), low-frequency (CF = 625 Hz) unit (no. 4/71715.PN) with a threshold of about 23 dB SPL. Data in rows 1, 2, and 3 correspond to stimulus frequencies f_T = 371 Hz (below CF), f_T = 625 Hz (at CF), and f_T = 918 Hz (above CF), respectively. Data in row 4 are for broad-band, periodically-reproduced Gaussian noise (with period T = 51.2 ms). In column 1, solid, dashed, and dotted curves represent stimulus levels of −20, 0, and +20 dB:FTC threshold, respectively. In column 2 solid and dashed curves represent stimulus levels of 30 and 50 dB:FTC threshold, respectively. For broad-band noise (row 4) the stimulus level cannot be related to the FTC threshold-values in a simple way. Roughly, the lowest level for noise is about −50 dB the FTC value at CF, and curves are presented in 20 dB increments. Plots of the PND count mean M (dotted curve), count variance V (dash-dot curve), and mean-to-variance ratio R (solid curve), versus stimulus level (dB:FTC), are presented in column 3. The stimulus level is varied from −20 to +70 dB in 10 dB steps. S represents spontaneous counts. Each PND shown consists of N_T = 250 samples, with T = 204.8 ms.

$R \leq 2$). The Fano factors for spontaneous PND's (Fig. 2) also fall in this range. The dependence of $F(T)$ on stimulus level for $T > 204.8$ ms remains to be determined.

C. Spontaneous PND's

The spontaneous T = 204.8 ms PND's associated with four units are presented in Fig. 2. They display the same irregularities evident in the driven PND's shown in Fig. 1. In this case the number of samples N_T = 500. The units have the following characteristics: (a) high-spontaneous, low-frequency unit (driven PND's for this unit are shown in Fig. 1); (b) high-spontaneous, high-frequency unit (PND's for this unit at CF are shown in [6, Fig. 6]); (c) high-spontaneous, low-frequency unit exhibiting spike pairs in the 51.2 ms PND; and (d) medium-spontaneous, high-frequency unit exhibiting spike pairs in the 51.2 ms PND (PND's for this unit at CF are shown in [6, Fig. 8]).

D. Dependence of the PND Statistics on Sample Size

The role of the number of samples (repetitions) N_T on the PND statistics is illustrated in Fig. 3 for a high-spontaneous, high-frequency unit with a CF of 12695 Hz. A pure-tone stimulus at 20 dB:re FTC (equivalent to 61 dB SPL) was applied to the unit at the CF. The upper-left panel displays the T = 51.2 ms PND collected with N_T = 1000 samples while the upper-right panel represents the T = 204.8 ms PND collected with N_T = 250 samples. The same neural spike train underlies both distributions. The PND in Fig. 3(a) is similar to those presented in [1] whereas the PND in Fig. 3(b) resembles those presented in Figs. 1 and 2 above.

In the lower pair of panels, all experimental conditions are identical except that N_T has been increased by a factor of 10 by extending the duration L of the experiment ($L = N_T T$) from 51.2 to 512 s. The means decrease and the Fano factors increase. In a separate series of experiments,

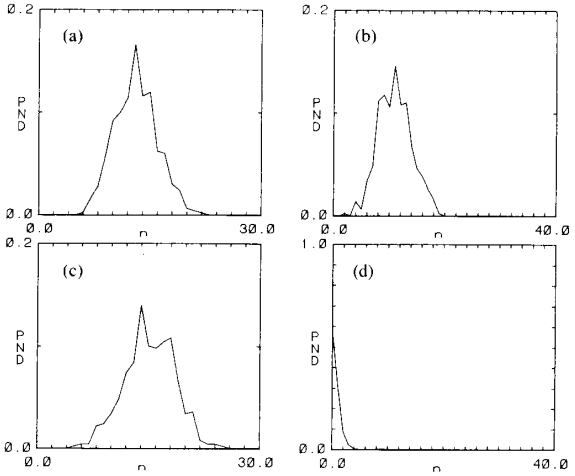

Fig. 2. Spontaneous long-counting-time PND's for four units. The number of samples $N_T = 500$ and $T = 204.8$ ms. In all cases the shapes of the spontaneous PND's show irregularities similar to those of the driven PND's. (a) Spontaneous PND for high-spontaneous, low-frequency unit No. 4/71715.PN. The driven PND's and PND statistics for this unit are displayed in Fig. 1. (b) Spontaneous PND for high-spontaneous, high-frequency unit no. 8/52304.PN. The PND's for this unit at CF are displayed in [6, Fig. 6]. (c) Spontaneous PND for high-spontaneous, low-frequency unit no. 7/72028.PN. (d) Spontaneous PND for medium-spontaneous, high-frequency unit no. 44/81426.PN. The PND's for this unit at CF are displayed in [6, Fig. 8].

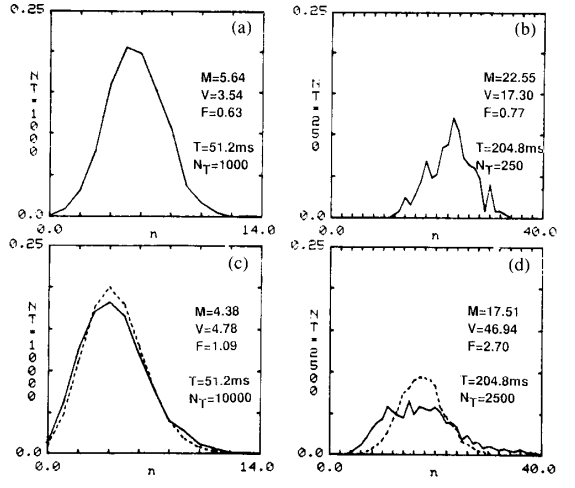

Fig. 3. PND's for a high-spontaneous, high-frequency (CF = 12695 Hz) unit (no. 5/42202.P4/P5) with a threshold of 41 dB SPL. The stimulus was a pure tone with level 20 dB : FTC at the CF (equivalent to 61 dB SPL). (a) $T = 51.2$ ms PND collected with $N_T = 1000$ samples ($L = 51.2$ s); (b) $T = 204.8$ ms PND collected with $N_T = 250$ samples ($L = 51.2$ s); (c) Solid curve is $T = 51.2$ ms PND collected with $N_T = 10\,000$ samples ($L = 512$ s) whereas dotted curve is simulated-Poisson distribution with the same mean and same N_T; (d) Solid curve is $T = 204.8$ ms PND collected with $N_T = 2500$ samples ($L = 512$ s) whereas dotted curve is simulated-Poisson distribution with same mean and same N_T. The PND's in (a) and (b) were constructed from the same underlying neural spike train, as were those in (c) and (d). Experimental values for the PND count mean M, count variance V, and variance-to-mean ratio F are specified in each of the panels.

we confirmed that for a given value of T (set at either 51.2 or 204.8 ms), M consistently decreased, and $F(T)$ consistently increased, as L increased from 512 ms through 5.12 to 25.6 s.

E. Accuracy of the PND Statistics

The expected variability of the PND resulting from the finite number of samples cannot be computed without knowledge of the underlying point process. For a homogeneous Poisson point process, with a sufficiently large number of samples, we have previously shown [1] that the standard deviation of the mean is $\Delta\langle n(T)\rangle \approx [\mathrm{Var}(n)/N_T]^{1/2}$ and the standard deviation of the mean-to-variance ratio is $\Delta R(T) \approx (2/N_T)^{1/2}$. The validity of these estimates was experimentally verified by conducting a laser-light experiment using a Langley–Ford model 1096 correlator/probability-analyzer to measure 50 photon-counting distributions ($N_T = 250$). Laser photon arrivals are well described by a homogeneous Poisson point process.

If the probabilities at different n are independent, the standard deviation for any probability value in the PND can be estimated by using the binomial probability law. Under this assumption, the standard deviation of any value of $p(n, T)$ is given by $\Delta p(n, T) \approx \{[p(n, T)][1 - p(n, T)]/N_T\}^{1/2}$.

The $T = 51.2$ ms PND presented in Fig. 3(c), which consists of $N_T = 10\,000$ samples, is not very different from the simulated-Poisson distribution with the same mean and number of samples (dotted curve). This is by chance of the choice of N_T. The short-counting-time PND's either have simple shapes, such as those shown in Fig. 3(a) and (c), or they exhibit an enhancement of even count-number probabilities. In either case, the shapes do not depend substantially on the number of samples (although the means do depend on N_T for runs in which the unit exhibits "fatigue").

However, comparing the $T = 204.8$ ms PND with $N_T = 250$ and 2500, in Fig. 3(b) and (d), respectively, illustrates an *increase* in the irregular nature of the PND, evidenced by the substantial increase in the Fano factor, as N_T increases. If the irregularities resulted from an insufficient number of samples, the Fano factor would *decrease* as N_T were increased. A simulated-Poisson distribution, of the same mean and number of samples [dotted curve in Fig. 3(d)], exhibits relatively small fluctuations and is, in fact, in reasonably good accord with the prediction of the independent-probability binomial rule, which gives $\Delta p(n, T) \approx 0.004$. The irregularities in the long-counting-time auditory-unit PND are substantially greater than either those of the simulated-Poisson distribution in Fig. 3(d) or the experimental PND in Fig. 3(a), even though N_T is larger in Fig. 3(d) than in Fig. 3(a).

We conclude that the irregular nature of the long-counting-time PND's does not arise from statistical inaccuracies associated with insufficient data, but rather from event clustering inherent in the auditory neural spike train.

TABLE I
EFFECT OF A LINEARLY DECREASING RATE ON THE PND STATISTICS FOR DATA PRESENTED IN FIG. 3[1]

Figure Number	T Counting Time (ms)	L Experimental Duration (s)	N_T Number of Samples	$\langle n \rangle$ Experimental Mean (M)	$F(T)$ Experimental Fano Factor	λ_{max} Maximum Rate (s^{-1})	λ_{min} Minimum Rate (s^{-1})	$F_{dec}(T)$ Linear-Decrease Fano Factor	$F_{res}(T)$ Residual (true) Fano Factor
(3a)	51.2	51.2	1000	5.64	0.63	112	108	0.001	0.63
(3b)	204.8	51.2	250	22.55	0.77	112	108	0.003	0.77
(3c)	51.2	512	10 000	4.38	1.09	108	63	0.10	0.99
(3d)	204.8	512	2500	17.51	2.70	108	63	0.40	2.30

[1]Use of an exponentially decreasing rate leads to nearly identical results.

F. Effects of Fatigue on the PND Statistics

In going from Fig. 3(a) to (c), and from (b) to (d), the count means decrease while the Fano factors increase. We demonstrate that a gradual decrease in the instantaneous rate of the spike train, usually ascribed to fatigue, cannot be responsible for either the large increase in the Fano factor or the irregularities in the PND's.

A useful model for fatigue is provided by an instantaneous rate λ_t that linearly decreases from a maximum value λ_{max} to a minimum value λ_{min} [10]. We consider an arbitrary counting distribution that has a Fano factor independent of its firing rate (this is representative of the T = 51.2 ms and 204.8 ms auditory PND's). The overall count mean $\langle n \rangle$, and Fano factor $F(T)$, can then be written as [11], [12]

$$\langle n \rangle = \tfrac{1}{2}(\lambda_{max} + \lambda_{min})T \tag{1}$$

and

$$F(T) = F_{res}(T) + (\lambda_{max} - \lambda_{min})^2 T/6(\lambda_{max} + \lambda_{min}), \tag{2}$$

respectively. The residual (true) Fano factor, $F_{res}(T)$, is obtained by subtracting the Fano factor contributed by the linearly decreasing mean, $F_{dec}(T)$ [represented by the second term in (2)], from the experimental Fano factor $F(T)$.

Results for the data illustrated in Fig. 3 are presented in Table I. The calculation was implemented by using the experimental mean count values for the T = 51.2 ms data represented in Fig. 3(a) and (c) (these data were collected sequentially), assuming that the mean pursued a linear decline through the two experiments. This enabled us to estimate the maximum instantaneous rate λ_{max} at the beginning of each experiment (after about $\frac{1}{2}$ s of stimulus application), and the minimum instantaneous rate λ_{min} at the end of each experiment, and thereby the "fatigue" contribution to the Fano factor $F_{dec}(T)$. We also carried out the same procedure for an exponentially (rather than linearly) decaying rate [13] and obtained numerical values virtually identical to those reported in Table I. Our calculations carry forward for an arbitrary direction of change in the instantaneous rate, including an increase, which often occurs if the measurement extends over a sufficiently long duration.

The results in Table I show that $F_{dec}(T)$ is negligible for the experiments with duration L = 51.2 s; this is also the case for L = 102.4 s. The residual Fano Factor $F_{res}(T)$ is essentially identical to the experimental Fano factor $F(T)$. We conclude that the irregularities in these PND's do not result from a systematically decreasing mean.

For the 512 s duration experiments, the values reported in Table I show that the linearly decreasing mean contributes ~ 15 percent to the Fano factor. Thus, the decreasing instantaneous rate accounts for only a small part of the increase in $F(T)$. The trend of increasing $F(T)$ with increasing T and N_T, manifested by the raw data, is left intact after corrections for the decreasing rate are incorporated, as evidenced by the behavior of $F_{res}(T)$.

Nevertheless, the hallmark of a linearly changing mean is visually apparent in the PND illustrated in Fig. 3(d). The smearing of the rate flattens the counting distribution at its top, much in the same way that a Poisson counting distribution with a linearly decreasing mean is flattened (see [11, Fig. 1] and [12, Fig. 4]). The high-count tail, on the other hand, reveals the presence of large intrinsic neural-spike clusters that are sufficiently rare to elude capture in experiments with a small number of samples but appear when N_T is sufficiently large.

G. Dependence of the Fano Factor on Counting Time

In Fig. 4(a) we present experimental results for the Fano factor $F(T)$, as a function of counting time T, for a range of counting times extending from 1 ms to 20 s. These data extend to greater counting times than those reported above. Values for the Fano factor versus counting time, like the variance-time curve [2], reveals information about correlations in the underlying sequence of events.

The very-short-duration data (T = 1 and 5 ms) were collected by Westerman [14]. He measured the evolution of the PND in gerbil primary auditory nerve fibers for 300 ms after the onset of a tone burst. The number of samples was N_T = 40. Although Westerman found that the instantaneous firing rate went through large changes during this 300 ms adaptation period, the Fano factor of the distribution for any given unit was found to either increase slightly during the adaptation (e.g., from $F(T) \approx 0.6$ to $F(T) \approx 0.8$) or to remain relatively constant. In this latter case, $F(T)$ ranged as low as 0.75 for some fibers and as high as unity for others.

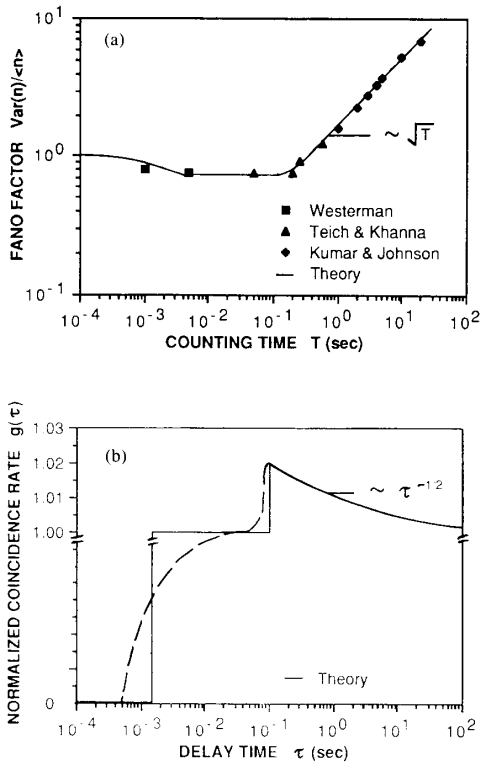

Fig. 4. (a) Fano factor $F(T)$ versus counting time T drawn from the data of Westerman [14], Teich and Khanna [1], [6], and Kumar and Johnson [15]. The solid curve is a plot of the theory represented in (5), which appears to properly characterize the data. $F(T) \sim \sqrt{T}$ for large T. (b) The dashed curve represents a plausible model for the normalized coincidence rate $g(\tau)$ versus delay time τ. It incorporates relative refractoriness at short delay times, independent neural firings at intermediate times, and power-law correlations at long delay times. $g(\tau) \sim 1/\sqrt{\tau}$ for large τ. The solid curve, which is the idealized version of $g(\tau)$ represented in (4), gives rise to the solid curve in (a).

The data with counting times between 51.2 and 563.2 ms were drawn from cat auditory-nerve-fiber PND's collected by Teich and Khanna [1], [6]. Typical values are indicated. The behavior of $F(T)$ for spontaneously firing and driven units apparently differs little. For units with CF's below a few kilohertz, where phase locking occurs, $F(T)$ was found to be relatively constant for T between 51.2 and 204.8 ms. (Phase locking may reduce the Fano factor slightly [1].) For units with CF's above several kilohertz, $F(T)$ increased in the characteristic way illustrated in Fig. 4(a).

The data with counting times between 1 and 20 s were recorded by Kumar and Johnson [15] from a spontaneously firing cat fiber (CF = 31.6 kHz, $\lambda \approx 24$ s^{-1}, L = 1132 s). Their study comprised only high-CF fibers, and the values of $F(T)$ varied from fiber to fiber. For this particular unit, the Fano factor increases in proportion to the square-root of counting time in the range 1.0 s $\leq T \leq$ 20 s. Kumar and Johnson did not calculate the Fano factor for $T >$ 20 s because of the low sample number.

III. Discussion

A. Evidence for Fractal Behavior in the Auditory Neural Spike Train

A number of experimental observations support the notion that auditory action potentials occur at fractal times, as indicated below.

1) An examination of Figs. 1–3 and [6, Figs. 6, 8, 9(a)] shows that *all* of the driven and spontaneous PND's with T = 204.8 ms have a rather irregular structure. The locations of the subpeaks differ in unpredictable ways for each experiment, including experiments conducted under identical conditions. This is true regardless of the spontaneous firing rate and CF of the unit, the stimulus frequency and intensity, the form of the stimulus (pure tones and reproducible Gaussian noise), and the number of samples. These subpeaks indicate that the probabilities of certain numbers of events are enhanced in any given experiment, i.e., that spike clusters of those sizes appear.

Berger and Mandelbrot [7], [8] long ago showed that random pairs and clusters of events appear in self-similar fractal point processes. These processes may be generated by randomizing a Cantor dust arranged in time (the dust then becomes a point process), or by a Lévy dust [7], [16]. The Brownian zeroset is the simplest Lévy dust, of fractal dimension $D = \frac{1}{2}$. A point process with fractal dimension between 0 and 1 may be generated in any number of ways.

2) The largest spike clusters exhibited in short-counting-time (T = 51.2 ms) PND's are spike pairs, manifested as an enhancement of even-count probabilities over odd-count probabilities [1, Figs. 8, 9, 12, 13]. As the counting time is increased, however, larger clusters appear in the PND's. This is reflected in an increase of the variance-to-mean ratio $F(T)$, which takes on a power-law form for sufficiently large T. The maximum cluster size appears to be limited by the counting time itself. The spike pairs, which are surely present since the short- and long-counting-time PND's are constructed from the same underlying spike train, disappear as T increases.

Random fractal point-processes exhibit a hierarchy of correlated spike occurrences that extends over multiple time scales, limited only by the duration of the sample. The pairs manifested in short-counting-time PND's are subclusters of larger clusters which appear in PND's with longer counting times, and so on, in nested fashion. Pairs are the smallest subclusters that are observable since refractoriness in the nerve fiber limits the production of tighter subclusters, i.e., refractoriness provides a lower limit for the inner cutoff [7], [8] of the fractal behavior. The presence of response correlations of long duration is also indicated by the results of Makeig *et al.* [17] on the evoked-response potential in the auditory system.

3) The number of large neural spike clusters increases not only with T, but also with the number of samples N_T, as is evident in the high-count tails of Fig. 3(b) and (d). The Fano factor therefore increases with increasing sample size, and does not appear to stabilize.

Large, but relatively rare, events contribute disproportionately to the variance and Fano factor of fractal processes. These contributions are associated with the long tails of the relevant probability distributions. The outlying events are sufficiently rare so that they elude capture in experiments in which N_T is small but they become increasingly evident, and indeed dominant, as the data collection time is extended.

4) The short-term average firing rate of spontaneous (and driven) activity is discontinuous and highly variable (see e.g., [15, Fig. 1]). The rate may follow a trend in which it consistently decreases, for example, only to suddenly reverse direction and consistently increase for a period of time.

Although behavior of this kind is often ascribed to a nonstationarity in the underlying process, this is proper only when the Gaussian central limit theorem is operative. This is not always the case. Fractal phenomena may be characterized by *stationary nonGaussian* (Lévy-stable) random variables and processes [7]. These distributions have long tails (that cause their variances to diverge) and provide excellent models for many diverse phenomena (e.g., price changes in economics) [7]. The trends that appear in such data can persist for very long times, but they can vanish as quickly as they set in. Mandelbrot [7] refers to the phenomena of persistence and discontinuity as the Joseph and Noah effects, respectively.

5) For low frequencies, the power spectral density of the short-term average firing rate takes the form $1/f^{\alpha}$ where f is the frequency and $0 < \alpha < 1$. Experimental spectral densities also exhibit sharp peaks at frequencies close to the inverse of the sample duration (see, e.g., [15, Appendix 2, Table II]).

A power spectral density of the form $1/f^{\alpha}$ (so-called $1/f$ or $1/f$-like noise) is a signature of the presence of multiple scales. The sample spectra of fractal random processes are broad but have sharp spectral peaks at frequencies close to the inverse of the duration of the data set [18].

B. Relation of Fano-Time Function and Normalized Coincidence Rate

We demonstrate that for an arbitrary stationary point process, power-law behavior for the Fano factor implies power-law behavior for the spike coincidence rate. We provide a plausible form for the coincidence rate that yields a Fano-time function which accords well with experiment. In the following section it is shown that the power spectral density of the spike train also assumes a power-law form in this case.

The Fano-time function is related to the probability density for event-pair coincidences $\lambda^2 g(\tau)$ by [2], [5], [19]:

$$F(T) = 1 + 2\lambda \int_0^T (1 - \tau/T)\left[g(\tau) - 1\right] d\tau \quad (3)$$

where λ is the mean rate of the point process and τ is the delay time. The normalized coincidence rate $g(\tau)$ plays the role of the correlation function for continuous processes.

A hypothetical, but plausible, normalized coincidence rate is indicated by the dashed curve in Fig. 4(b). The slowly rising portion of the curve represents the effects of relative refractoriness [20]; spikes cannot occur more closely than the absolute refractory period ($\approx \frac{1}{2}$ ms). After the refractoriness period is over, the curve spends a brief time in the vicinity of unity, where the event occurrences are uncorrelated. For delay times longer than ≈ 40 ms, the coincidence rate increases above unity, representing correlation of the spike occurrences for long delay times. These long-delay correlations are responsible for the appearance of spike clusters in the PND.

The solid curve in Fig. 4(b) represents an idealization of these effects that enables us to readily calculate $F(T)$ from $g(\tau)$ using (3). A Poisson process modified by fixed nonparalyzable dead time τ_d [2], [5], [19] exhibits a normalized coincidence rate that is zero for $\tau < \tau_d$ and approximately unity[2] for $\tau \geq \tau_d$. Excess coincidences ($g(\tau) > 1$), representing fractal behavior, set in at delay times of the order of the fractal characteristic time of the system τ_f. The idealized normalized coincidence rate is chosen to be

$$g(\tau) = \begin{cases} 0 & \tau < \tau_d \\ 1 & \tau_d \leq \tau \leq \tau_f \\ 1 + \delta(\tau/\tau_f)^{-1/2} & \tau > \tau_f \end{cases} \quad (4)$$

where δ is a constant and the inverse square-root-law is selected to provide agreement with the Fano-time function, as indicated below. The solid curve in Fig. 4(b) is a plot of (4) with the neurophysiologically plausible values $\tau_d = 1.5$ ms, $\lambda = 98\ \text{s}^{-1}$, $\tau_f = 0.1$ s, and $\delta = 0.02$.

Using (4) in (3) leads to

$$F(T) = \begin{cases} 1 - \lambda T & T < \tau_d \\ 1 - \lambda\tau_d[2 - \tau_d/T] & \tau_d \leq T \leq \tau_f \\ 1 - \lambda\tau_d[2 - \tau_d/T] + \frac{8}{3}\delta\lambda\tau_f\left[(T/\tau_f)^{1/2}\right. & \\ \quad \left. + \frac{1}{2}(\tau_f/T) - \frac{3}{2}\right], & T > \tau_f \end{cases} \quad (5)$$

which is shown as the solid curve in Fig. 4(a). The Fano-time curve calculated from the coincidence rate in (3) is seen to agree well with the data. The theoretical curve takes on the value unity at $T = 0$; as T increases it plateaus at a constant value below unity, as for a dead-time-modified Poisson process. The square-root growth of the Fano factor for large T, $F(T) \sim (T/\tau_f)^{1/2}$, follows from the delay-time dependence of the coincidence rate for large τ, $g(\tau) \sim (\tau/\tau_f)^{-1/2}$, as promised.

[2]The approximation is satisfactory for values of $\lambda\tau_d$ appropriate for neural refractoriness. The exact formula, which is provided and plotted in [5, (A29), Fig. 11(b)], reveals the presence of damped oscillations in the coincidence rate for $\tau \geq \tau_d$.

More generally, if the Fano factor increases with T in fractional-power-law fashion with exponent α ($0 < \alpha < 1$),

$$F(T) \sim (T/\tau_f)^{\alpha}, \qquad \tau_f \leq T \leq \tau_{f'} \tag{6}$$

it is clear from (3) that

$$g(\tau) \sim (\tau/\tau_f)^{\alpha-1} \qquad \tau_f \leq \tau \leq \tau_{f'}. \tag{7}$$

Thus, fractional-power-law behavior for the Fano factor and coincidence rate accompany each other.

C. Spectrum of the Auditory Neural Spike Train

The frequency spectrum (power spectral density) of a random process $S(f)$ is determined from its coincidence rate by means of the Wiener–Khinchine theorem. When $g(\tau)$ takes the form indicated in (7), $S(f)$ behaves as

$$S(f) \sim f^{-\alpha} \qquad f_{f'} \leq f \leq f_f \tag{8}$$

in the low-frequency (large delay-time) regime. The quantity f_f is the cutoff frequency associated with τ_f. When $\alpha = \frac{1}{2}$, as in (4) and (5), $S(f) \sim f^{-1/2}$ (0.05 Hz $\leq f \leq$ 10 Hz). At yet lower frequencies, the spectral density of the spike train may move toward an approximately $1/f$ character [21], with α approaching unity in that region.

D. Fractal Dimension of the Auditory Neural Spike Train

The fractal dimension D is a measure of the degree of event clustering, or irregularity of a sequence of events, that is preserved over different time scales [7]. It falls between the topological dimension $D_T = 0$ and the Euclidian dimension $E = 1$ [7]. We therefore take D for the auditory neural spike train to be the exponent α in the Fano factor $F(T)$ as given in (6). As indicated above, α therefore uniquely determines the power-law falloff of the coincidence rate and the spectral density of the process.

If values for the Fano factor are known at two counting times, T_1 and T_2, D may be estimated from (6) as

$$D \approx \log\left[F(T_2)/F(T_1)\right]/\log\left(T_2/T_1\right). \tag{9}$$

We have used this formula to calculate D for several primary auditory nerve fibers and found values lying between 0.3 and 0.9, for counting times in the range 0.2 s $\leq T \leq$ 0.55 s. These values are similar to those applicable for the German federal telephone network ($D \approx 0.3$) and other similar channels ($0.2 < D < 1$) [7]. For the data presented in Fig. 4, $D \approx \frac{1}{2}$ for 0.1 s $\leq T <$ 20 s.

E. Comparison of Auditory, Optic, Vestibular, and Poisson PND's

Neural spike clusters are also known to be present in cat optic-nerve fibers at low light levels [22]–[26]; in striate cortex neurons [27], [28]; in the nervous system of crustaceans [27], [29, and references therein], [30]; and in preparations such as the squid giant axon periodically forced by a sinusoidal current [31].

The fractal dimension D of the retinal-ganglion-cell spike train can be estimated from two dark pulse-number distributions published by Barlow and Levick [23, Fig. 5] for a particular fiber. The probability density function in [23, Fig. 5] yields the following values for the means and Fano factors of the two distributions: $M_1 = 0.32$ and $F(T_1) = 1.2425$ for $T_1 = 0.1$ s; $M_2 = 3.23$ and $F(T_2) = 1.441828$ for $T_2 = 1.0$ s. Using (9) gives $D \approx 0.06$. From a number of indications, temporal fractal behavior appears to be less prevalent in optic-nerve fibers than in auditory nerve fibers: optic-nerve firings often exhibit exponential tails in the PID [26] and their firings become progressively more regular as the luminance increases. Unlike auditory-nerve firings, at high stimulus levels $F(T)$ becomes independent of T [22] so that $D = 0$. The spontaneous firings of some striate cortex neurons [28, Fig. 1], on the other hand, appear to be fractal, at least from visual inspection.

As a distinct counterpoint to the clusters that appear in the neural spike trains of all primary auditory fibers, the data for a spontaneously firing low-skew vestibular unit is illustrated in Fig. 5. It is well known that such units fire in a far more regular pattern than do auditory units [32]; their firing pattern is similar to that of optic nerve fibers at high luminance levels. In Fig. 5(a) and (b) we present short-counting-time ($T = 51.2$ ms, $N_T = 2000$) and long-counting-time ($T = 204.8$ ms, $N_T = 500$) spontaneous vestibular PND's, respectively, for one such unit. Both of these PND's were constructed from the same neural spike train. They exhibit PND count means $M(51.2$ ms$) = 1.95$ and $M(204.8$ ms$) = 7.81$, respectively, and (very low) Fano factors $F(51.2$ ms$) = 0.04$ and $F(204.8$ ms$) = 0.03$, respectively. The small values of $F(T)$ indicate that these vestibular nerve firings tick along with the near regularity of a clock.

In Fig. 5(c) we present the PID for this same unit. This PID is the usual unscaled version $P^{(1)}(t)$ [3] which represents the probability density of the time intervals between adjacent events. The number of samples is 2000 and the resolution of the time axis is 0.2 ms (8 bins). The large narrow peak indicates that the time between adjacent spikes is almost always 27 ± 3 ms (note the expanded abscissa). The sample mean interspike interval $\langle t^{(1)} \rangle = 26.9$ ms and the interspike-interval coefficient of variation $CV^{(1)} = 0.0449$. Based on the classification provided by Walsh *et al.* [32], this spike train arises from a low-skew vestibular unit.

Finally, in Fig. 6 we present a comparison of the PND's for vestibular, auditory, and simulated-Poisson data with the same approximate spike rate ($\lambda \approx 40$ s^{-1}). Short-counting-time PND's ($T = 51.2$ ms) are shown in Fig. 6(a) and long-counting-time PND's ($T = 204.8$ ms) are shown in Fig. 6(b). The vestibular data (denoted VES) are the same as those shown in Fig. 5. The auditory data (denoted AUD) are drawn from Unit 7/72028.PN, stimulated by a pure tone of frequency 1445 Hz and of level -20 dB: re FTC [1, Fig. 8]. This particular data set was chosen because its spike rate was quite close to that of the

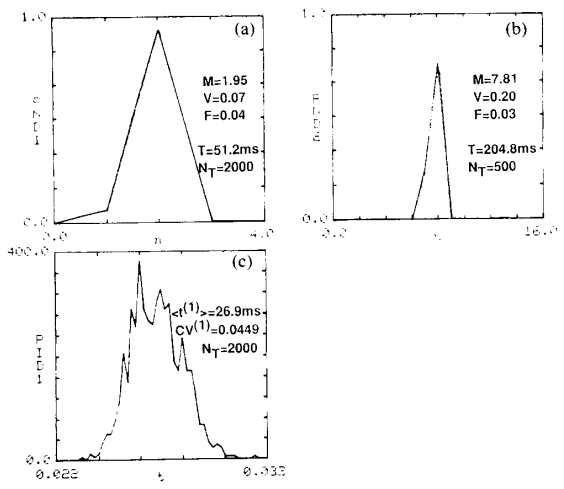

Fig. 5. Short- and long-counting-time PND's, and PID, for a low-skew vestibular unit (No. 14/72027.P4). All three distributions are very narrow, illustrating the regularity in the firing pattern. (a) $T = 51.2$ ms PND collected with $N_T = N = 2000$ samples; (b) $T = 204.8$ ms PND collected with $N_T = 500$ samples; (c) PID collected with 2000 samples (note expanded abscissa). The PND's in (a) and (b) were constructed from the same underlying neural spike train. Experimental values for the PND count mean M, count variance V, and variance-to-mean ratio F are specified in the PND panels. Experimental values for the sample mean interspike interval $\langle t^{(1)} \rangle$ and the interspike-interval coefficient of variation $CV^{(1)}$ are specified in the PID panel.

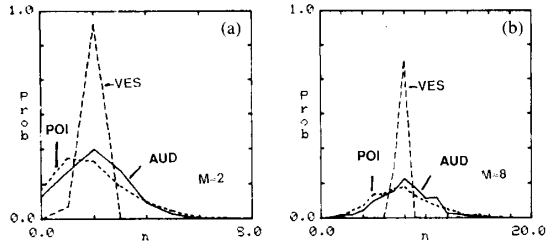

Fig. 6. Comparison of PND's for vestibular, auditory, and simulated-Poisson data with the same approximate spike rate (≈ 40/s). Short-counting-time PND's ($T = 51.2$ ms) are shown in (a); long-counting-time PND's ($T = 204.8$ ms) are shown in (b). The vestibular data (denoted VES) are drawn from unit no. 14/72027.P4; see Fig. 5. The vestibular PND count means in (a) and (b) are $M(51.2\text{ ms}) = 1.95$ and $M(204.8\text{ ms}) = 7.81$, respectively, and its variance-to-mean ratios in (a) and (b) are $F(51.2\text{ ms}) = 0.04$ and $F(204.8\text{ ms}) = 0.03$, respectively. The auditory data (denoted AUD) are drawn from unit no. 7/72028.PN, stimulated by a pure tone of frequency 1445 Hz and level -20 dB : re FTC (see [1, Fig. 8]). The auditory PND count means in (a) and (b) are $M(51.2\text{ ms}) = 2.01$ and $M(204.8\text{ ms}) = 8.03$, respectively, and its variance-to-mean ratios in (a) and (b) are $F(51.2\text{ ms}) = 0.70$ and $F(204.8\text{ ms}) = 0.81$, respectively. The simulated-Poisson (denoted POI) count means in (a) and (b) are $M(51.2\text{ ms}) = 1.92$ and $M(204.8\text{ ms}) = 7.85$, respectively, and its variance-to-mean ratios in (a) and (b) are $F(51.2\text{ ms}) = 1.02$ and $F(204.8\text{ ms}) = 1.08$, respectively. The vestibular and auditory PND's in (a) and (b) were constructed from the same underlying neural spike train. $N_T = 2000$ and 500 for the short- and long-counting-time vestibular PND's, respectively, whereas $N_T = 1000$ and 250 for the short- and long-counting-time auditory and simulated-Poisson PND's. The vestibular PND's are clearly the narrowest, the simulated-Poisson PND's the broadest, and the auditory PND's the most irregular.

vestibular unit. The simulated-Poisson data (denoted POI) were calculated by means of a C language program written for the AT&T 3B2 computer and a Basic-language program written for the IBM PC. The vestibular PND's are clearly the narrowest and the simulated-Poisson PND's the broadest. However, it is the auditory PND's that are the most irregular.

IV. Conclusion

A. Nature and Usefulness of the PND

The behavior of the PND is most readily captured by its count mean M and variance-to-mean ratio $F(T)$. The count mean is directly proportional to the usual rate function for the unit. The form and magnitude of $F(T)$ provide measures for the regularity of the underlying spike train. If events are generally well organized along the time axis, the Fano factor will be small (as it is for the vestibular unit) since the numbers of events in successive intervals of duration T are relatively constant. If random pairs or spike clusters appear, the Fano factor will be large since a cluster will sometimes be captured in an interval of duration T and sometimes not. For the zero-memory homogeneous Poisson process, $F(T) = 1$ for all T whereas for the highly regular pulse train, $F(T) \to 0$ for sufficiently large T [5]. Very-short-time PND measurements tend to cut apart both clusters and regularity, and result in a low-mean, Poisson-like distribution. This is because refractoriness restricts the possible outcomes to be either 0 spikes or 1 spike in this case, which gives rise to the Bernoulli distribution [5].

There are a number of practical reasons why the PND is useful for compiling neural data [1]: 1) time jitter and time quantization in the measurement system become unimportant so that PND data are not contaminated by these instrumental effects (the PID and PST can suffer from such limitations); and 2) it provides a statistically valid measure for studying units that fire at low rates. Under these conditions it is difficult to collect a statistically significant PID or PST histogram.

B. Fractal Nature of the Auditory Point Process

Probably most important, the PND provides the experimenter with a useful window on the coding of information. In primary auditory fibers it has revealed temporal fractal behavior taking the form of nested sequences of spike clusters.

It is desirable to seek a mathematical model for the point process that reflects the underlying physiological behavior of the system. The PND's are quite well fit by the reduced-quintinomial distribution [6], but this is principally a phenomenological construct. A number of models would appear to give rise to a fractal point process. We believe that several of these merit further study: 1) models in which the haircell gives rise to a fractal presynaptic signal, e.g., neurotransmitter release may be governed by fractal ionic channel openings and closings[3]; 2) models in which the diffusion of neurotransmitter across the synaptic junction obeys fractal dynamics; 3) random-walk models involving excitatory and inhibitory steps at the

[3]We have found that a simple inverse power-law, $p^{(1)} \sim 1/t$, fits some channel transition histograms remarkably well.

postsynaptic junction, such as those considered by Gerstein and Mandelbrot [33]; and 4) models in which chaotic oscillations of the membrane potential [34] may initiate action potentials [31] with fractal characteristics. We are investigating the possibilities of casting some of these models in the form of a sick-time-modified doubly stochastic Poisson point process [35]. The stochastic rate takes on a fractal character and exhibits a correlation function that gives rise to the Fano-time function reported in Section III-B.

Why would the auditory action potentials exhibit fractal behavior and the vestibular units not? Since the auditory neural spike train serves to sample slowly varying envelope information [36], we suggest that these unusual auditory neural-firing patterns may serve to efficiently sample natural fractal noises. Indeed, the instantaneous audio power of music and speech, and the instantaneous frequency (rate of zero crossings) of music, exhibit $1/f$ noise over a substantial range of low frequencies [37]. An analogous argument for the visual system would suggest that fractal neural firings might be present at loci where image information is sampled, e.g., at the striate cortex. The potential benefits to be gained from such sampling, such as bandwidth compression, require examination from an information-theoretic point of view. The vestibular system, in contrast, does not sample an information-carrying signal but rather estimates angular acceleration with high accuracy. This task, it seems, would be best served by a sequence of regularly firing nonfractal action potentials.

C. Fractal Behavior in the Nervous System

The presence of spike pairs and clusters in the nervous system is greeted with skepticism by some and with enthusiasm by others. More than one auditory neurophysiologist has said that the pairs must be an artifact resulting from recording near a node of Ranvier. Other neurophysiologists, working with different preparations, have ascribed significant signal processing significance to them [28], [38]. Spike pairs and clusters can simply arise, as we have shown, from action potential occurrences at fractal times. Such behavior may be quite prevalent. Further investigation of where fractal behavior occurs may lead to further understanding of why fractal behavior occurs in the nervous system.

Acknowledgment

I am grateful to S. Keilson, S. Khanna, and S. Lowen of Columbia University for helpful suggestions. I thank D. Johnson of Rice University for sharing some of his unpublished spectral data and for useful discussions. I appreciate the help of many undergraduate and graduate students in writing software and conducting experiments: D. Feld, C. Goldberg, P. Guiney, I. Storper, T. Tanabe, R. Turcott, and L. Young.

References

[1] M. C. Teich and S. M. Khanna, "Pulse-number distribution for the neural spike train in the cat's auditory nerve," *J. Acoust. Soc. Amer.*, vol. 77, pp. 1110–1128, 1985; ——, "Pulse-number distribution for the neural discharge in the cat's auditory nerve," *J. Acoust. Soc. Amer. Suppl. 1*, vol. 71, p. S17, 1982; ——, "Behavior of the pulse-number distribution for the neural spike train in the cat's auditory nerve," *J. Acoust. Soc. Amer. Suppl. 1*, vol. 74, p. S7, 1983.

[2] D. R. Cox and P. A. W. Lewis, *The Statistical Analysis of Series of Events*. London: Methuen, 1966.

[3] R. W. Rodieck, N. Y-S. Kiang, and G. L. Gerstein, "Some quantitative methods for the study of spontaneous activity of single neurons," *Biophys. J.*, vol. 2, pp. 351–368, 1962.

[4] G. L. Gerstein and N. Y-S. Kiang, "An approach to the quantitative analysis of electrophysiological data from single neurons," *Biophys. J.*, vol. 1, pp. 15–28, 1960.

[5] M. C. Teich, B. E. A. Saleh, and J. Peřina, "Role of primary excitation statistics in the generation of antibunched and sub-Poisson light," *J. Opt. Soc. Amer. B*, vol. 1, pp. 366–389, 1984.

[6] M. C. Teich and R. G. Turcott, "Multinomial pulse-number distributions for neural spikes in primary auditory fibers: Theory," *Biol. Cybern.*, vol. 59, pp. 91–102, 1988.

[7] B. B. Mandelbrot, *The Fractal Geometry of Nature*. New York: Freeman, 1983.

[8] J. M. Berger and B. B. Mandelbrot, "A new model of error clustering on telephone circuits," *IBM J. Res. Dev.*, vol. 7, pp. 224–236, 1963; B. B. Mandelbrot, "Self-similar error clusters in communication systems and the concept of conditional stationarity," *IEEE Trans. Commun. Tech.*, vol. 13, pp. 71–90, 1965.

[9] M. C. Teich, "Fractal character of the auditory neural spike train," *J. Acoust. Soc. Amer.*, suppl. 1, vol. 84, p. S55, 1988.

[10] R. V. Harrison, "Long-term adaptation in afferent neurones from the normal and pathological cochlea," *J. Acoust. Soc. Amer. Suppl. 1*, vol. 77, p. S94, 1985.

[11] M. C. Teich and P. Diament, "Flat counting distribution for triangularly modulated Poisson process," *Phys. Lett.*, vol. 30A, pp. 93–94, 1969.

[12] P. R. Prucnal and M. C. Teich, "Statistical properties of counting distributions for intensity-modulated sources," *J. Opt. Soc. Amer.*, vol. 69, pp. 539–544, 1979.

[13] B. Lütkenhöner and R. L. Smith, "Rapid adaptation of auditory-nerve fibers: Fine structure at high stimulus intensities," *Hearing Res.*, vol. 24, pp. 289–294, 1986.

[14] L. A. Westerman, "Adaptation and recovery of auditory nerve responses," Tech. Rep. ISR-S-24, Inst. Sensory Res., Syracuse Univ., Syracuse, NY, Jan. 1985; L. A. Westerman and R. L. Smith, "Adaptation and variability of spike discharge of auditory nerve," *J. Acoust. Soc. Amer. Suppl. 1*, vol. 75, p. S13, 1984.

[15] A. Kumar and D. Johnson, "The applicability of stationary point process models to discharge patterns of single auditory-nerve fibers," Tech. Rep. 84-09, Rice Univ., Houston, TX, November 1984; D. H. Johnson and A. Kumar, "Analysis of the stationarity of models of auditory-nerve fiber discharge patterns," *J. Acoust. Soc. Amer. Suppl. 1*, vol. 77, p. S93, 1985.

[16] B. B. Mandelbrot, "Renewal sets and random cutouts," *Z. für Wahrscheinlichkeitstheorie*, vol. 22, pp. 145–157, 1972.

[17] S. Makeig, R. Galambos, and D. R. Stapells, "Studies of the auditory steady-state response I. Minute-rhythms," *J. Acoust. Soc. Amer. Suppl. 1*, vol. 77, p. S65, 1985.

[18] B. B. Mandelbrot and J. W. Van Ness, "Fractional Brownian motions, fractional noises and applications," *SIAM Rev.*, vol. 10, pp. 422–437, 1968.

[19] M. C. Teich and B. E. A. Saleh "Photon bunching and antibunching," *Progr. Opt.*, vol. 26, pp. 1–104, 1988.

[20] P. R. Gray, "Conditional probability analyses of the spike activity of single neurons," *Biophys. J.*, vol. 7, pp. 759–777, 1967; R. P. Gaumond, C. E. Molnar, and D. O. Kim, "Stimulus and recovery dependence of cat cochlear nerve fiber spike discharge probability," *J. Neurophysiol.*, vol. 48, pp. 856–873, 1982.

[21] D. H. Johnson, Rice Univ., private communication.

[22] H. B. Barlow and W. R. Levick, "Three factors limiting the reliable detection of light by the retinal ganglion cells of the cat," *J. Physiol., (London)*, vol. 200, pp. 1–24, 1969.

[23] ——, "Changes in the maintained discharge with adaptation level in the cat retina," *J. Physiol. (London)*, vol. 202, pp. 699–718, 1969.

[24] H. B. Barlow, W. R. Levick, and M. Yoon, "Responses to single quanta of light in retinal ganglion cells of the cat," *Vision Res.*, vol. 11, suppl. 3, pp. 87–101, 1971.

[25] D. N. Mastronarde, "Correlated firing of cat retinal ganglion cells. II. Responses of X and Y cells to single quantal events," *J. Neurophysiol.*, vol. 49, pp. 325–349, 1983.

[26] B. E. A. Saleh and M. C. Teich, "Multiplication and refractoriness in the cat's retinal-ganglion-cell discharge at low light levels," *Biol. Cybern.*, vol. 52, pp. 101-107, 1985.
[27] J. E. Dayhoff and G. L. Gerstein, "Favored patterns in spike trains. I. Detection," *J. Neurophysiol.*, vol. 49, pp. 1334-1348, 1983; "Favored patterns in spike trains. II. Application," *J. Neurophysiol.*, vol. 49, pp. 1349-1363, 1983.
[28] C. R. Legéndy and M. Salcman, "Bursts and recurrences of bursts in the spike trains of spontaneously active striate cortex neurons," *J. Neurophysiol.*, vol. 53, pp. 926-939, 1985.
[29] N. Sugano, "Effect of doublet impulse sequences in the crayfish claw opener muscles and the computer-simulated neuromuscular synapse," *Biol. Cybern.*, vol. 49, pp. 55-61, 1983.
[30] A. V. Holden and W. Winlow, "Neuronal activity as the behavior of a differential system," *IEEE Trans. Syst., Man, Cybern.*, vol. SMC-13, pp. 711-719, 1983.
[31] K. Aihara and G. Matsumoto, "Chaotic oscillations and bifurcations in squid giant axons," in *Chaos*, A. V. Holden Ed. Princeton, NJ: Princeton Univ., 1986, pp. 257-269.
[32] B. T. Walsh, J. B. Miller, R. R. Gacek, and N. Y-S. Kiang, "Spontaneous activity in the eighth cranial nerve of the cat," *Int. J. Neurosci.*, vol. 3, pp. 221-236, 1972.
[33] G. L. Gerstein and B. B. Mandelbrot, "Random walk models for the spike activity of a single neuron," *Biophys. J.*, vol. 4, pp. 41-68, 1964.
[34] T. R. Chay and J. Rinzel, "Bursting, beating, and chaos in an excitable membrane model," *Biophys. J.*, vol. 47, pp. 357-366, 1985.
[35] B. E. A. Saleh and M. C. Teich, "Multiplied-Poisson noise in pulse, particle, and photon detection," *Proc. IEEE*, vol. 70, pp. 229-245, 1982; B. E. A. Saleh, J. T. Tavolacci, and M. C. Teich, "Discrimination of shot-noise-driven Poisson processes by external dead: Application to radioluminescence from glass," *IEEE J. Quantum Electron.*, vol. QE-17, pp. 2341-2350, 1981.
[36] M. C. Teich and S. M. Khanna, in preparation.
[37] R. F. Voss and J. Clarke, " '1/f noise' in music: Music from 1/f noise," *J. Acoust. Soc. Amer.*, vol. 63, pp. 258-263, 1978.
[38] W. R. Klemm and C. J. Sherry, "Serial ordering in spike trains: What's it 'trying to tell us'?," *Int. J. Neurosci.*, vol. 14, pp. 15-33, 1981.

Malvin C. Teich (S'62-M'66-SM'72-F'89) was born in New York City. He received the S.B. degree in physics from the Massachusetts Institute of Technology, Cambridge, MA, in 1961, the M.S. degree in electrical engineering from Stanford University, Stanford, CA, in 1962, and the Ph.D. degree in quantum electronics from Cornell University, Ithaca, NY, in 1966.

In 1966 he joined the M.I.T. Lincoln Laboratory, Lexington, MA, where he was engaged in work on coherent infrared detection. In 1967, he became a member of the faculty in the Department of Electrical Engineering, Columbia University, New York, where he is now teaching and pursuing his research interests in the areas of quantum optics, photonics, optical and infrared detection, and sensory perception. He served as Chairman of the Department from 1978 to 1980. He is also a member of the faculty in the Department of Applied Physics, and a member of the Columbia Radiation Laboratory, the Center for Telecommunications Research, and the Fowler Memorial Laboratory at the Columbia College of Physicians & Surgeons. He has authored or coauthored some 150 technical publications and holds one patent.

Dr. Teich is a member of Sigma Xi, the American Physical Society, the Optical Society of America, the Acoustical Society of America, the Society for Neuroscience, the American Association for the Advancement of Science, and the New York Academy of Sciences. He served as a member of the Editorial Advisory Panel for *Optics Letters* from 1977 to 1979. In 1969 he was the recipient of the IEEE Browder J. Thompson Memorial Prize for his paper "Infrared heterodyne detection" and in 1981 he received the Citation Classic Award of *Current Contents* for this work. He was appointed a Fellow of the John Simon Guggenheim Memorial Foundation in 1973, was elected a Fellow of the Optical Society of America in 1983, and a Fellow of the American Physical Society in 1988. He is currently a member of the Board of Editors of the journal *Quantum Optics*.